ADVANCED MATERIALS
www.advmat.de

www.MaterialsViews.com

3D-Printing of Lightweight Cellular Composites

*Brett G. Compton and Jennifer A. Lewis**

Lightweight cellular composites, composed of an interconnected network of solid struts that form the edges or faces of cells,[1] are an emerging class of high-performance structural materials that may find potential application in high stiffness sandwich panels,[2] energy absorbers,[3] catalyst supports,[4] vibration damping,[5] and insulation.[6] They offer several advantages due to their low density, high specific properties,[7] and potential for multifunctionality.[8,9] The most ubiquitous cellular composite is wood, which not only supports substantial self-weight and wind loading, but efficiently transports nutrients over long distances to sustain growth. By controlling composition and architecture over multiple length scales, natural materials are able to achieve remarkable properties from biological polymers, e.g., cellulose and lignins. Balsa wood is a prime example, which rivals the best engineering materials in terms of specific bending stiffness, $E^{1/2}/\rho$, and specific bending strength, $\sigma^{2/3}/\rho$.[10]

Here, we report a new epoxy-based ink that enables 3D printing of cellular composites with controlled alignment of multi-scale, high aspect ratio fiber reinforcement to create hierarchical structures inspired by balsa wood (**Figure 1**a). 3D printing offers unparalleled flexibility in achieving controlled composition, geometric shape, function, and complexity over traditional manufacturing methods.[11,12] However, despite continuing advances, there are few examples that fully leverage the potential of additive manufacturing to create fiber-reinforced composite architectures[13] or use structural matrices, such as epoxy resins.[14] Using this unique combination of hierarchical inks and 3D printing, we create lightweight, wood-inspired cellular composites that cannot be fabricated any other way. These materials exhibit Young's modulus values that are an order of magnitude higher than those obtained by thermoplastics and photocurable resins developed for commercial 3D printing methods, while retaining comparable strength.

Our 3D extrusion printing method has been used previously to fabricate ceramic, metallic, and polymeric scaffolds,[15,16] 3D antennae and sensors,[14,17,18] and rechargeable Li ion microbatteries,[19] with features ranging from microns to millimeters in size. Central to this process is the design of concentrated viscoelastic inks that exhibit significant shear thinning to allow extrusion through micronozzles under ambient conditions without requiring prohibitively high printing pressures. However, after exiting the nozzle, they possess sufficiently high shear elastic modulus, G', and shear yield strength, τ_y, to maintain their printed filamentary shape. By carefully tailoring the ink composition and rheology, we can control the printability, architecture, and properties of patterned 3D structures.

To fabricate lightweight cellular composites, we first create epoxy-based inks that embody the essential rheological properties required for our 3D printing method. Unlike prior ink designs that undergo solidification via gelation, drying, or on-the-fly photopolymerization,[12,14,15,18] epoxy resins are reactive materials that initially exhibit a low viscosity, which rises over time as the reaction proceeds under ambient conditions. Moreover, these inks ultimately require thermal curing at elevated temperatures (100–220 °C) for several hours to complete the polymerization process. We created epoxy-based inks that exhibit the desired viscoelasticity and long pot-life in the absence and presence of highly anisotropic fillers. Specifically, we formulated the base epoxy inks using an Epon 826 epoxy resin, nano-clay platelets, and dimethyl methyl phosphonate (DMMP). The nano-clay platelets (1 nm thick; 100 nm in length) primarily serve as a rheology modifier that imparts both shear thinning behavior and a shear yield stress to the uncured ink, while DMMP serves to reduce the initial viscosity of the resin to allow higher solids loading. Both of these additives may also enhance the mechanical properties of the cured epoxy matrix.[20–23] Next, we added silicon carbide whiskers (0.65 μm in diameter; 12 μm mean length) and carbon fibers (10 μm in diameter; 220 μm mean length) to the base formulation to create fiber-filled, epoxy inks. These high aspect ratio fillers align under the shear and extensional flow field that develops within the micronozzle during printing[13,24–27] (Figure 1b), resulting in enhanced stiffening in the cured composite along the printing direction. Finally, we used an imidazole-based ionic liquid as a latent curing agent to greatly extend the printing window (i.e., 30-day pot-life) under ambient conditions. This approach effectively decouples the printing process from the curing process and enables inks to print consistently over the course of several weeks. Imidazole-based curing agents are also known to impart chemical stability and heat resistance to epoxy

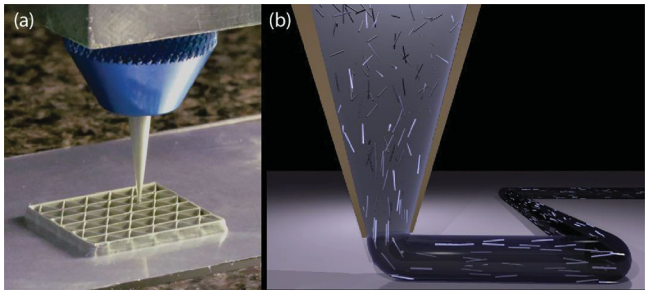

Figure 1. (a) Optical image of 3D printing of a triangular honeycomb composite. (b) Schematic illustration of the progressive alignment of high aspect ratio fillers within the nozzle during composite ink deposition.

Dr. B. G. Compton, Prof. J. A. Lewis
School of Engineering and Applies Sciences
Wyss Institute for Biologically Inspired Engineering
Harvard University Cambridge
MA 02318, USA
E-mail: jalewis@seas.harvard.edu

DOI: 10.1002/adma.201401804

resins.[28–30] The properties of these individual constituents as well as representative ink formulations are provided in Table S1 and S2, respectively.

The rheological behavior of epoxy-based inks of varying composition are shown in **Figure 2**. The pure epoxy resin with DMMP exhibits a viscosity (η) of ~1.5 Pa•s that is independent of shear rate (Figure 2a). As a consequence, the shear storage modulus (G') of this ink is lower than its loss modulus (G''), and both moduli are independent of applied shear stress (Figure 2b). While the resin readily flows through fine nozzles under modest applied pressures, it immediately wets and spreads upon exiting the nozzle and lacks the ability to support itself. The addition of nano-clay platelets transforms the resin into a viscoelastic fluid. The resulting material, referred to as the base epoxy ink, possesses a η that exceeds 10^4 Pa•s at low shear rates (~0.01 s^{-1}) that is four orders of magnitude higher than the pure resin. Due to its strong shear thinning behavior, this ink exhibits an apparent viscosity of ~20 Pa•s at shear rates (~50 s^{-1}) typically experienced during printing. Hence, the ink viscosity is only an order of magnitude higher than that of the resin alone under relevant printing conditions. The base epoxy ink exhibits a plateau value of G' ~10^4 Pa that exceeds G'' by about an order of magnitude at low stress. At the crossover point between the two moduli curves, its shear yield stress (τ_y) is ~150 Pa. Upon adding SiC whiskers to the base epoxy ink to create a SiC-filled epoxy ink, the viscosity increases by approximately an order of magnitude at a given shear rate without altering its shear thinning behavior. At the characteristic shear rate of 50 s^{-1}, the SiC-filled epoxy ink viscosity is ~200 Pa•s. Finally, the addition of large carbon fibers (10% by weight of resin) to the SiC-filled epoxy ink (refered to as the SiC/C-filled epoxy ink) has little effect on either the ink viscosity or degree of shear thinning. However, the incorporation of SiC whiskers and carbon fibers to the base epoxy ink increases the G' and τ_y to ~7×10^5 Pa, and 4×10^3 Pa, respectively. Due to their high stiffness and yield stress, these inks are ideally suited for 3D printing of cellular composites. Moreover, given their solid-like nature in the quiescent state, the filler species within these inks undergo minimal aggregation or sedimentation.

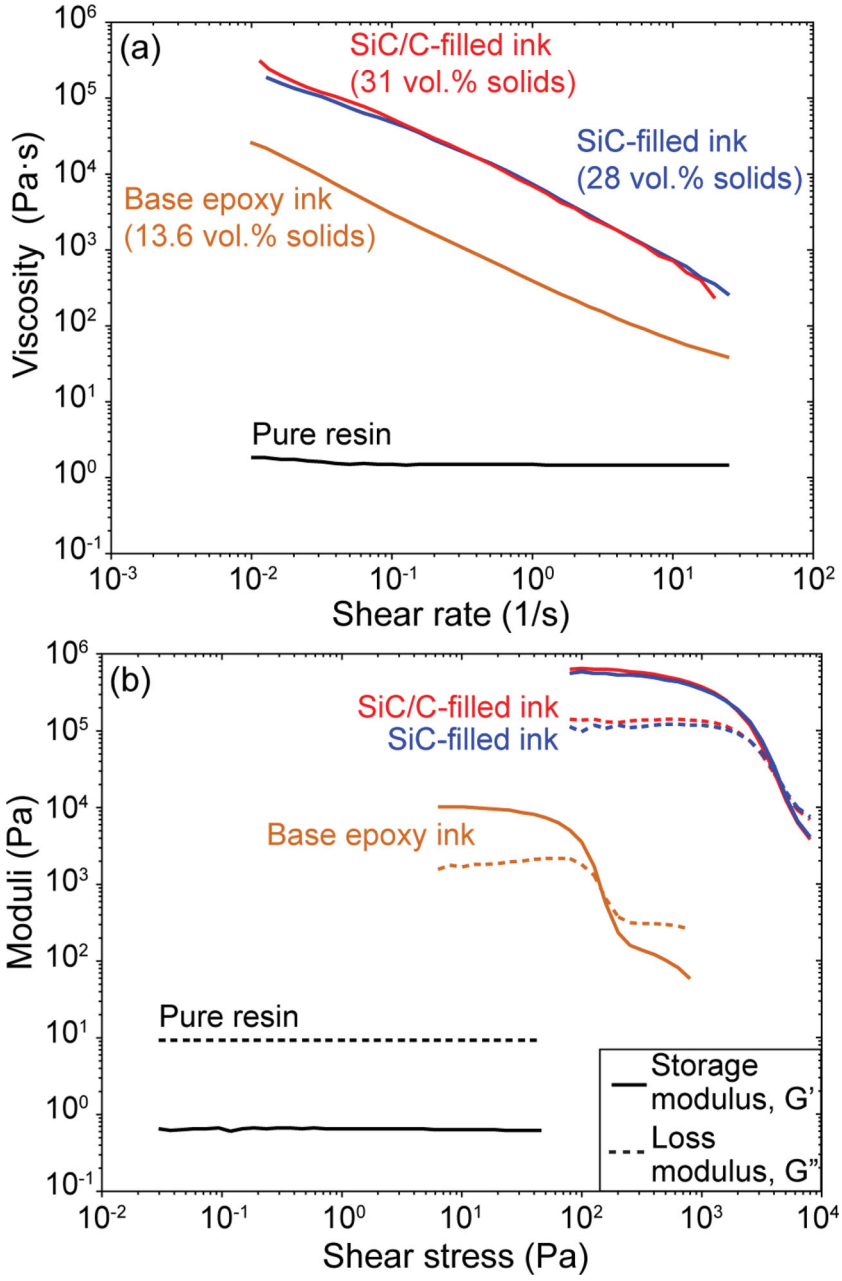

Figure 2. Log-log plots of (a) apparent viscosity as a function of shear rate and (b) shear storage and loss moduli as a function of shear stress for epoxy-based inks of varying composition.

To investigate the effects of shear-induced filler alignment, we printed tensile bars with different printing paths – one oriented longitudinally along the tensile direction and the other oriented transverse to the tensile direction (Figure S1). The results are shown in **Figure 3** along with tensile data for specimens printed using the base epoxy ink (without SiC whiskers or carbon fiber fillers). Printed composites show a substantial increase in Young's modulus, E, over the pure resin from 2.66 ± 0.17 GPa to 10.61 ± 1.38 and 8.06 ± 0.45 GPa for the SiC-filled and SiC/C-filled transverse specimens, respectively, and 16.10 ± 0.03 and 24.5 ± 0.83 GPa for the SiC-filled and SiC/C-filled longitudinal specimens, respectively. These values represent up to a 9x increase in the Young's modulus over cast samples composed of pure epoxy resin. Failure strength values, σ_f, for the printed composites are comparable to that of the cast epoxy resin samples (71.1 ± 5.3 MPa), with the longitudinal specimens exhibiting somewhat higher strengths (96.6 ± 13.8 and 66.2 ± 6.1 MPa, for the SiC-filled

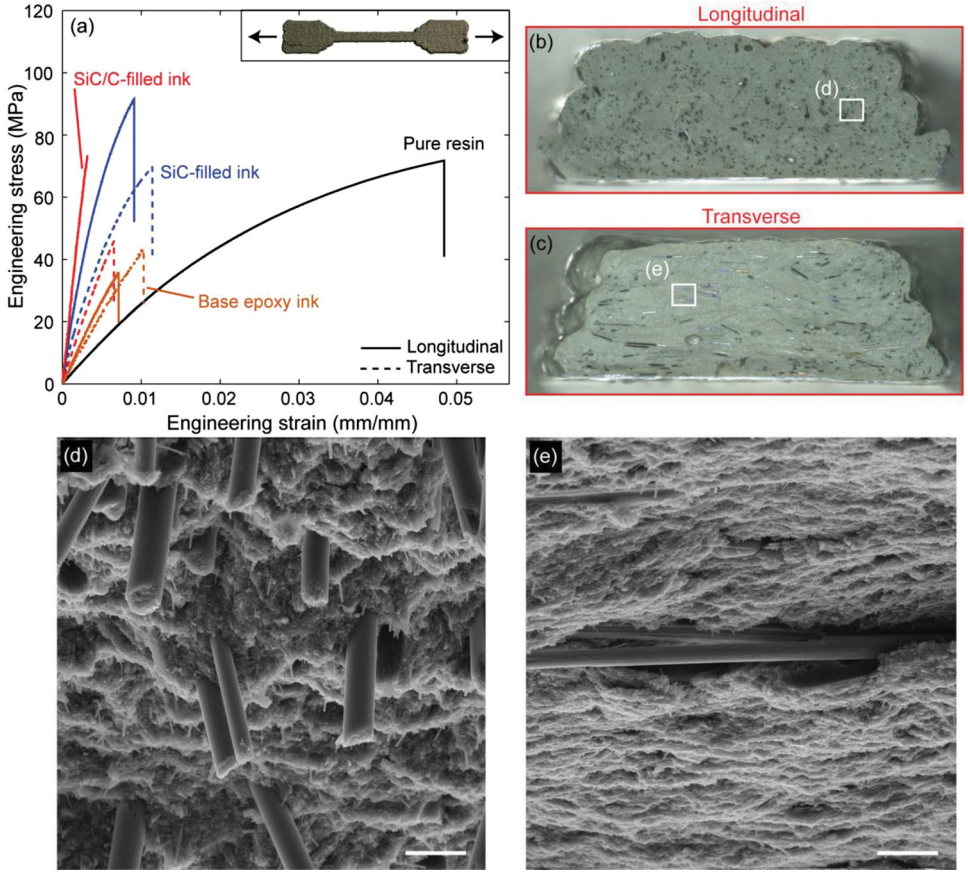

Figure 3. (a) Representative tensile stress versus strain curves for 3D printed tensile bars of varying composition and control samples cast from pure epoxy resin. Tensile fracture surfaces of longitudinally and transversely printed SiC/C-filled specimens at (b, c) low and (d,e) higher magnification, respectively. Scale bars in (d) and (e) are 20 μm.

and SiC/C-filled composites, respectively) than the transverse specimens for both filled epoxy inks (69.8 ± 2.9 and 43.9 ± 4.1 MPa, for the SiC-filled and SiC/C-filled composites, respectively). The control samples produced using the base epoxy ink possess isotropic properties independent of build direction with nearly identical values of $E = 6.22 \pm 0.49$ and 5.55 ± 0.97 GPa and $\sigma_f = 29.2 \pm 4.8$ and 33.6 ± 10.1 MPa for longitudinal and transverse specimens, respectively. The mechanical properties for these three samples are summarized in Table S3. Interestingly, only a small decrease in properties is observed when these inks are printed using a larger nozzle (610 μm diameter) (Figure S2), which may not be statistically significant given the standard deviation. While both nozzle sizes induce fiber alignment throughout the printed filaments, we anticipate that above a critical nozzle size, whose value increases with printing speed, the fibers would only align in yielded regions near the nozzle walls, where the shear stress exceeds the ink's shear yield stress.

The tensile fracture surfaces do not show any evidence of the original printed filaments, indicating full coalescence of the filaments during deposition, and minimal evidence of deposition-related defects (e.g., bubbles, nozzle clogging, or filament debonding) (Figure 3b,c). SEM micrographs of the fracture surfaces also highlight the multi-scale reinforcement active in these composites (Figure 3d-e). The anisotropic fillers align with printing direction – both the SiC whiskers and carbon fibers each display significant pullout in the longitudinal specimens and minimal pullout in the transverse specimens. Hence, we can exploit fiber pullout, a well known toughening mechanism, simply by controlling the printing path.

To demonstrate 3D printing of cellular composites, we created several architectures with varying cell geometry, as shown in **Figure 4**. The 3D structures shown in Figure 4a-c are produced by printing the SiC-filled epoxy ink through a 200 μm nozzle. These high aspect ratio, cellular structures possess a wall thickness of roughly 200 μm and exceed 2 mm in height (~20 layers thick). The representative structure shown in Figure 4d-f is produced by printing the SiC/C-filled epoxy ink using a 410 μm nozzle. The cell walls of this structure are nominally 350 μm thick. Within each cell wall, the large carbon fibers are clearly visible and highly aligned along the printing direction. The high degree of shear induced alignment enables carbon fibers whose length exceeds both the nozzle size and cell wall thickness to be reliably printed without clogging. Additional images of this structure and a translucent honeycomb composite are provided in Figure S3 and S4, respectively, along with a movie (Movie S1) that highlights the fabrication of the translucent composite.

To quantify their mechanical properties, we subjected the triangular honeycomb structures to in-plane compression tests for samples printed with a range of cell sizes and relative

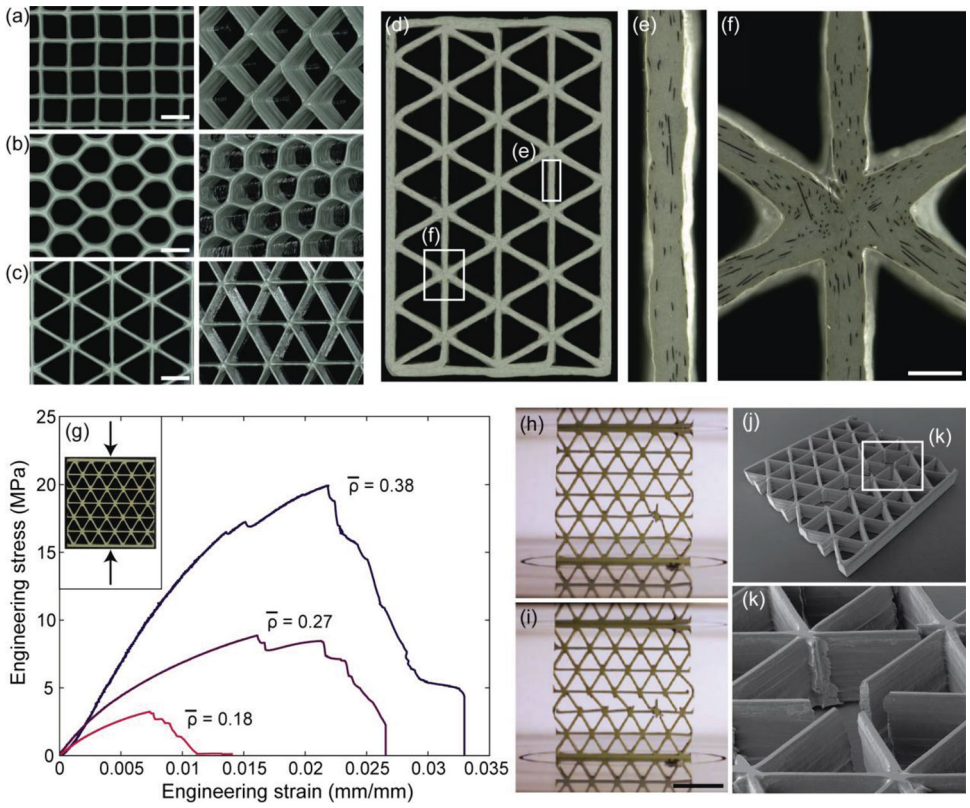

Figure 4. Optical images of (a) square, (b) hexagonal, and (c) triangular honeycomb structures composed of SiC-filled epoxy. Scale bars are 2 mm. (d-f) Optical images of a triangular honeycomb structure composed of SiC/C-filled epoxy, which reveal highly aligned carbon fibers oriented along the print direction. The scale bars in (e-f) are 500 μm. (g) Representative compressive stress versus strain curves for printed triangular honeycomb structures over a range of relative densities. Still images from video acquired during mechanical testing show an initial node rotation failure event (h), followed by damage propagation from that site in the form of elastic wall buckling and tensile fracture (i). The scale bars for (h-i) are 10 mm. (j-k) SEM images of the failure site show an imperfection in the cell wall, which may have led to the initial node rotation.

densities. Representative stress-strain curves are shown in Figure 4g, which display incremental load drops that correspond to discrete failure events highlighted in still frames taken from videos acquired during testing (Figure 4h,i). The failure modes include elastic wall buckling, node rotation, and tensile failure of the cell walls. The site of one node rotation is shown in the SEM images in Figure 4j,k. Results are discarded from any test where out of plane buckling is observed.

The Young' modulus and strength values for triangular honeycombs are plotted in **Figure 5**. The scaling laws governing the elastic modulus and strength of cellular materials are well established:[31]

$$\frac{E}{E_s} = B\left(\frac{\rho}{\rho_s}\right)^b \tag{1}$$

and

$$\frac{\sigma_c}{\sigma_{TS}} = C\left(\frac{\rho}{\rho_s}\right)^c \tag{2}$$

where E_s, σ_{TS}, and ρ_s are the Young's modulus, tensile strength, and density of the base solid material, respectively, and E and σ_c are the Young's modulus and strength, respectively. For a triangular lattice, $B = C = 1/3$ and $b = 1$. The value of the exponent c depends on the nature of failure in the material: $c = 1$ when the cell walls fail in uniaxial tension or compression, and $c = 2$ when the cell walls fail via elastic buckling. It is important to note that the mechanical properties of cellular structures are not dependent on their absolute size, but depend solely on the properties of the base material, architecture, and relative density. These 3D cellular composites therefore benefit from design aspects inspired by balsa wood (e.g., cellular architecture coupled with multi-scale, aligned reinforcement) without having to reproduce such features at the specific length scales observed in wood. Model predictions are plotted in Figure 5 using properties measured for the SiC/C-filled epoxy composites. We find that the modulus values closely follow the expected linear scaling with density, albeit at roughly half the predicted value, and the strength values closely follow the scaling law indicative of failure via wall buckling, in agreement with observations made during the tests (Figure 4h,i). The cellular structures are somewhat stronger than the predictions based on tensile strength data. This observation may be attributed to erroneously low tensile strength values due to stress concentrators in the tensile samples, or to size effects due to the specific flaw populations in the composites. The discrepancy between observed and predicted modulus values, as well as the propensity for failure via buckling of the cell walls, can be attributed, in part,

ADVANCED MATERIALS
www.advmat.de

www.MaterialsViews.com

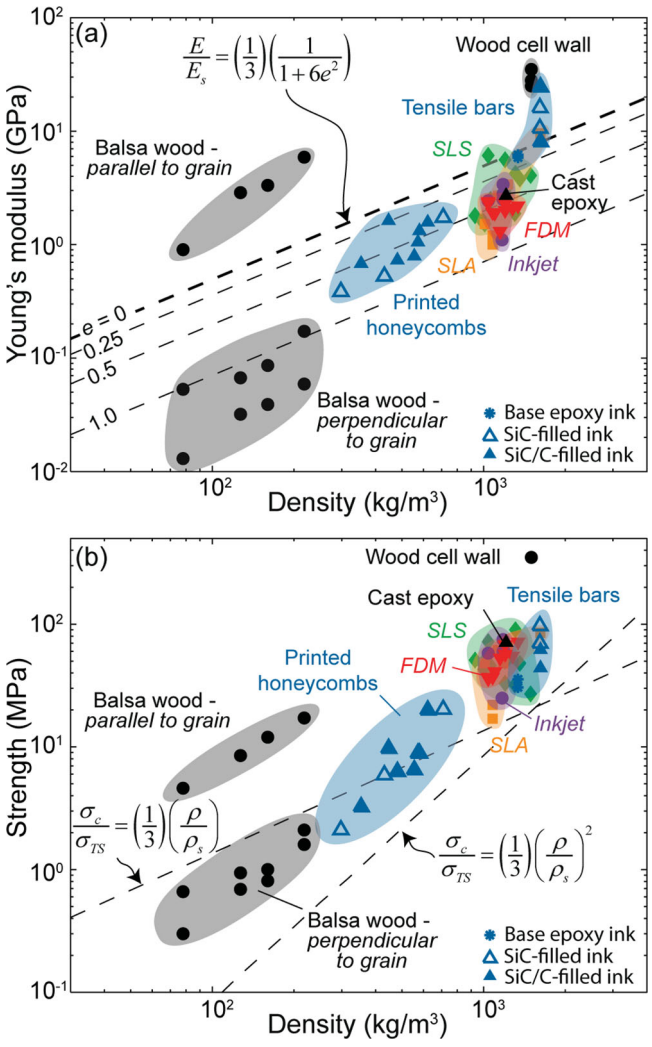

Figure 5. (a) Property space maps of Young's modulus versus density and (b) strength versus density, which compare our printed epoxy-based composites to polymers and polymer composites fabricated by commercial 3D printing methods and to balsa wood.[9] Analytical predictions are plotted as dashed lines using properties of the SiC/C-filled composite. Measured honeycomb modulus data match predictions for geometric imperfections on the order of $\ell \approx 0.25-0.5$, while strength data follow the scaling law for failure via buckling. [Note: Commercial data sources are provided in the SI.]

to geometric imperfections in the lattice structure, including nodal misalignment (Figure S3c) and waviness in the cell walls, which have been observed in the printed structures (Figure S5). Following analyses by Symons and Fleck,[32] and Grenestedt,[33] the modulus of a triangular honeycomb structure with wavy imperfections in the cell walls is given by:

$$\frac{E}{E_s}=\left(\frac{1}{3}\right)\left(\frac{\rho}{\rho_s}\right)\left(\frac{1}{1+6\ell^2}\right) \quad (3)$$

where $e \equiv w_0/t$, and w_0 is the amplitude of waviness and t is the wall thickness. Predictions for reduced modulus values are plotted in Figure 5a for various values of e, and it can be seen that good agreement is observed for $e \approx 0.5$. The occurence of such defects is a sensitive function of ink stiffness and strength, wall aspect ratio, and deposition parameters, and is likely to increase with lower relative density structures.

As a benchmark, we have plotted the mechanical properties of 3D printed commercial polymers and polymer composites as well as balsa wood and wood cell walls alone alongside our results in Figure 5. Tensile bars printed using our SiC/C-filled epoxy inks exhibit longitudinal Young's modulus values nearly equivalent to wood cell walls, 10–20x higher than most commercial, 3D printed polymers, and 2x higher than the best commercial printed polymer composites. Hence, our composites are competitive with both wood and commercial 3D printed structures in terms of absolute stiffness. Indeed, because our cellular honeycomb composites can be printed in a triangular motif with very high in-plane fiber alignment rather than the nominally hexagonal motif found in balsa wood, their in-plane properties are approximately 3x to 8x better than the transverse properties (perpendicular to the grain) of balsa wood at the same density. Moreoever, our printed composite cellular structures offer the added benefits of being isotropic in-plane, where wood is not[10,31] and exhibit equivalent modulus values as bulk printed polymers at half the density.

In summary, we have demonstrated the first 3D printed cellular composites composed of oriented fiber-filled epoxy with exceptional mechanical properties. Because alignment of high aspect ratio fillers occurs along the print direction, the build path itself can be used to spatially control their orientation within the part. This capability adds an entirely new dimension to engineering design and optimization, where composition, stiffness, and toughness within a bulk 3D object can be digitally integrated with component design to achieve a highly optimized structure. For example, reinforcements could be aligned around geometric stress concentrators or stiffness could be graded near fixture points to minimize damage. In addition to creating structures that mimic balsa wood, our approach is ideally suited to fabricate a wide range of bio-inspired composite structures with controlled architecture and mechanical properties.

Experimental Section

Epoxy-Based Inks: The inks are prepared by mixing an epoxy resin (Epon 826 epoxy resin, Momentive Specialty Chemicals, Inc., Columbus, OH) with appropriate amounts of dimethyl methyl phosphonate (DMMP, Sigma Aldrich, St. Louis, MO), nano-clay platelets (Cloisite 30b, Southern Clay Products, Inc., Gonzales, TX), silicon carbide whiskers (SI-TUFF SC-050, ACM, Greer, SC), and milled carbon fibers (Dialead K223HM, Mitsubishi Plastics, Inc., Tokyo, Japan) using a Thinky Planetary Centrifugal Mixer (Thinky USA, Inc., Laguna Hills, CA) in a 125 mL glass container using a custom adaptor. An imidazole-based ionic liquid is employed as a latent curing agent (Basionics VS03, BASF Intermediates, Ludwigshafen, Germany). The properties of individual constituents are given in Table S1.

Batches started with 30 g of Epon 826 resin. 3 g of DMMP are added, followed by 2 minutes of mixing in the Thinky mixer. Next, SiC whiskers are added in 5 or 10 g increments, followed by nano-clay platelets in 2 g increments. When used, the milled carbon fibers are added in 1 g increments. After adding each constituent to the ink, it is mixed for 3–5 min in the Thinky mixer. Finally, the ink is allowed to cool to room temperature prior to the addition of the curing agent, Basionics VS03, at 5 wt% of the total epoxy resin added. When carbon fibers are

COMMUNICATION

used, 0.5 g of acetone is added along with the curing agent. After the addition of the curing agent, the ink is mixed for additional 3 minutes.

Ink Rheology: Rheological properties of the ink are characterized using an AR 2000ex Rheometer (TA Instruments, New Castle, DE) with a 40 mm flat plate geometry and a gap of 500 μm for the base and SiC-filled epoxy inks and 1000 μm for the SiC/C-filled ink. All measurements are preceded by a one minute conditioning step at a constant shear rate of 1 s^{-1}, followed by a ten minute rest period to allow the ink structure to reform.

3D Printing: The inks are loaded into 3 cc, luer-lock syringes (Nordson EFD, Westlake, OH) and centrifuged at 3900 rpm for 10 minutes to remove bubbles. Loaded syringes are then mounted in an HP3 high-pressure adaptor (Nordson EFD), which is placed on an Aerotech 3-axis positioning stage (Aerotech, Inc., Pittsburgh, PA). Ink is driven pneumatically and controlled via an Ultimus V pressure box (Nordson EFD), which interfaces with the Aerotech motion control software. Luer-lock syringe tips (Nordson EFD) are used to dictate filament diameter, and inks are printed onto glass slides covered with Bytac, PTFE-coated aluminum foil (Saint Gobain Performance Plastics, Worcester, MA) to prevent adhesion. Print paths for each geometry are written as parameterized g-code scripts and designed to maximize continuity within each printed layer. Printed parts are pre-cured at 100 °C for 15 h, cooled, removed from the substrate, and cured for 2 h at 220 °C.

Characterization: Density measurements on fully cured samples are made using the Archimedes method, and the relative density of honeycombs specimens is calculated from the measured mass and volume of each specimen. Prior to testing, surfaces of the honeycomb specimens are ground flat to ensure good contact with the compression platens. Printed specimens are tested in an Instron 5566 load frame (Instron, Norwood, MA) at a nominal rate of 2.0×10^{-4} s^{-1}. Strain in the samples is measured using the Instron Advanced Video Extensometer (AVE). Reported tensile properties represent an average of at least three samples.

Supporting Information

Supporting Information is available from the Wiley Online Library or from the author.

Acknowledgements

The authors gratefully acknowledge generous support from the BASF North American Center for Research on Advanced Materials (NORA), headed by Dr. Marc Schroeder. JAL also acknowledges support from the Harvard MRSEC (NSF DMR 0820484). We would like to thank Profs. Lorna Gibson and Alan Lesser for helpful discussions related to this work as well as Drs. James Weaver and Lori Sanders for assistance with sample imaging.
Note: Equation 2 was corrected after initial publication online.

Received: April 21, 2014
Revised: May 12, 2014
Published online: June 18, 2014

[1] L. J. Gibson, M. F. Ashby, *Cellular solids: structure and properties*, Cambridge university press, **1999**.
[2] F. W. Zok, H. Rathbun, M. He, E. Ferri, C. Mercer, R. M. McMeeking, A. G. Evans, *Philos. Mag.* **2005**, *85*, 3207.
[3] C. I. Hammetter, R. G. Rinaldi, F. W. Zok, *J. Appl. Mech.-Trans. ASME* **2013**, *80*.
[4] W. M. Carty, P. W. Lednor, *Curr. Opin. Solid State Mat. Sci.* **1996**, *1*, 88.
[5] J. Banhart, J. Baumeister, M. Weber, *Mater. Sci. Eng., A* **1996**, *205*, 221.
[6] J. Kuhn, H. P. Ebert, M. C. Arduinischuster, D. Buttner, J. Fricke, *Int. J. Heat Mass Transf.* **1992**, *35*, 1795.
[7] M. F. Ashby, *Philos. Trans. R. Soc., A* **2006**, *364*, 15.
[8] A. G. Evans, J. W. Hutchinson, N. A. Fleck, M. F. Ashby, H. N. G. Wadley, *Prog. Mater. Sci.* **2001**, *46*, 309.
[9] H. N. G. Wadley, *Philos. Trans. R. Soc., A*, **2006**, *364*, 31.
[10] L. J. Gibson, *J. R. Soc. Interface* **2012**, *9*, 2749.
[11] G. Kim, Y. Oh, Proc. Inst. Mech. Eng., B: *Journal of Engineering Manufacture* **2008**, *222*, 201.
[12] D. T. Pham, R. S. Gault, *Int. J. Mach. Tools Manuf.* **1998**, *38*, 1257.
[13] M. L. Shofner, K. Lozano, F. J. Rodriguez-Macias, E. V. Barrera, *J. Appl. Polym. Sci.* **2003**, *89*, 3081.
[14] R. D. Farahani, H. Dalir, V. Le Borgne, L. A. Gautier, M. A. El Khakani, M. Levesque, D. Therriault, *Nanotechnology* **2012**, *23*.
[15] S. Ghosh, S. T. Parker, X. Y. Wang, D. L. Kaplan, J. A. Lewis, *Adv. Funct. Mater.* **2008**, *18*, 1883.
[16] J. L. Simon, S. Michna, J. A. Lewis, E. D. Rekow, V. P. Thompson, J. E. Smay, A. Yampolsky, J. R. Parsons, J. L. Ricci, *J. Biomed. Mater. Res., Part A* **2007**, *83A*, 747.
[17] J. J. Adams, E. B. Duoss, T. F. Malkowski, M. J. Motala, B. Y. Ahn, R. G. Nuzzo, J. T. Bernhard, J. A. Lewis, *Adv. Mater.* **2011**, *23*, 1335.
[18] S. Z. Guo, F. Gosselin, N. Guerin, A. M. Lanouette, M. C. Heuzey, D. Therriault, *Small* **2013**, *9*, 4118.
[19] K. Sun, T.-S. Wei, B. Y. Ahn, J. Y. Seo, S. J. Dillon, J. A. Lewis, *Adv. Mater.* **2013**, *25*, 4539.
[20] P. C. LeBaron, Z. Wang, T. J. Pinnavaia, *Appl. Clay Sci.* **1999**, *15*, 11.
[21] J. H. Park, S. C. Jana, *Macromolecules* **2003**, *36*, 2758.
[22] R. A. Riggleman, J. F. Douglas, J. J. de Pablo, *Soft Matter* **2010**, *6*, 292.
[23] A. S. Zerda, A. J. Lesser, *J. Appl. Polym. Sci.* **2002**, *84*, 302.
[24] J. P. Bell, *J. Compos. Mater.* **1969**, *3*, 244.
[25] M. Farkash, D. G. Brandon, *Mater. Sci. Eng., A* **1994**, *177*, 269.
[26] K. Langhans, E. Roeder, *Materialwiss. Werkstofftech.* **1992**, *23*, 174.
[27] K. N. Murty, G. F. Modlen, *Polym. Eng. Sci.* **1977**, *17*, 848.
[28] A. Farkas, P. F. Strohm, *J. Appl. Polym. Sci.* **1968**, *12*, 159.
[29] M. Heise, G. Martin, *Macromolecules* **1989**, *22*, 99.
[30] M. Ito, H. Hata, K. Kamagata, *J. Appl. Polym. Sci.* **1987**, *33*, 1843.
[31] N. A. Fleck, V. S. Deshpande, M. F. Ashby, *Proc. R. Soc. A* **2010**, *466*, 2495.
[32] D. D. Symons, N. A. Fleck, *J. Appl. Mech.-Trans. ASME* **2008**, 75.
[33] J. L. Grenestedt, *J. Mech. Phys. Solids* **1998**, *46*, 29.